

# Layer-By-Layer Assembly of Asymmetric Linkers into Non-Centrosymmetric Metal Organic Frameworks: A Thorough Theoretical Treatment

Modan Liu, David Elsing, Meysam Esmailpour, Mariana Kozłowska, Wolfgang Wenzel,\* and Christof Wöll\*

Layer-by-layer synthesis of surface-coordinated metal–organic frameworks (SURMOF) enables the assembly of asymmetric, dipolar linkers into non-centrosymmetric pillar-layered structures. Using appropriate substrate terminations can yield oriented growth with the dipoles aligned perpendicular to the surface. The aligned pillar linkers give rise to a built-in electrostatic field. In addition, the non-centrosymmetric structure of the SURMOF gives rise to intriguing nonlinear optical features, such as second harmonic generation. Previous research with methyl-functionalized bipyridine pillar linkers have demonstrated that this approach works in principle, but so far the total degree of alignment is only very small. Herein, a multiscale modelling approach is presented for in-silico SURMOF assembly to identify and overcome limitations in the growth of pillar-layered SURMOFs and to develop a strategy to maximize linker alignment. Using master equation models and kinetic Monte Carlo simulations, it is found that the formation of a highly ordered state corresponding to the thermodynamic equilibrium is often prevented by long-lasting transient effects. Based on *ab initio* binding energies for a wide selection of hypothetical pillar linkers, a fast-binding, slow-relaxation scheme is able to be identified during the SURMOF growth for a range of different pillar linkers. These observations allow them to derive a rational strategy for the design of novel linkers to yield SURMOF-based non-centrosymmetric materials with substantially improved properties.

## 1. Introduction

Non-centrosymmetric (NC) solid-state materials are of particular interest due to their unique properties, such as piezoelectricity, ferroelectricity, and even-order nonlinear optical effects (NLO).<sup>[1,2]</sup> The advantageous properties of NC compounds due to intrinsic static electric fields are directly related to the absence of spatial inversion symmetry. In nature, only a few inorganic materials, such as ZnO, KH<sub>2</sub>PO<sub>4</sub>, LiNbO<sub>3</sub>, and KTiOPO<sub>4</sub>, exhibit intrinsic electric fields and nonlinear optical properties that originate from their distinct, NC crystalline structures.<sup>[3,4]</sup> Inspired by their natural counterparts, researchers have investigated approaches to engineer NC materials from designed inorganic and organic compounds, which exhibit superior NLO performance.<sup>[2,5]</sup>

In this study we investigated metal-organic heterostructures with regard to their propensity to engineer NC properties into a highly ordered 3D structure. Such tunability of the alignment is of particular interest for applications of layered

M. Liu, C. Wöll  
Institute of Functional Interfaces (IFG)  
Karlsruhe Institute of Technology  
Hermann-von-Helmholtz-Platz 1, 76344 Eggenstein-Leopoldshafen,  
Germany  
E-mail: christof.woell@kit.edu

D. Elsing, M. Esmailpour, M. Kozłowska, W. Wenzel  
Institute of Nanotechnology  
Karlsruhe Institute of Technology  
Hermann-von-Helmholtz-Platz 1, 76344 Eggenstein-Leopoldshafen,  
Germany  
E-mail: wolfgang.wenzel@kit.edu

 The ORCID identification number(s) for the author(s) of this article can be found under <https://doi.org/10.1002/adfm.202302516>

© 2023 The Authors. Advanced Functional Materials published by Wiley-VCH GmbH. This is an open access article under the terms of the Creative Commons Attribution License, which permits use, distribution and reproduction in any medium, provided the original work is properly cited.

DOI: 10.1002/adfm.202302516

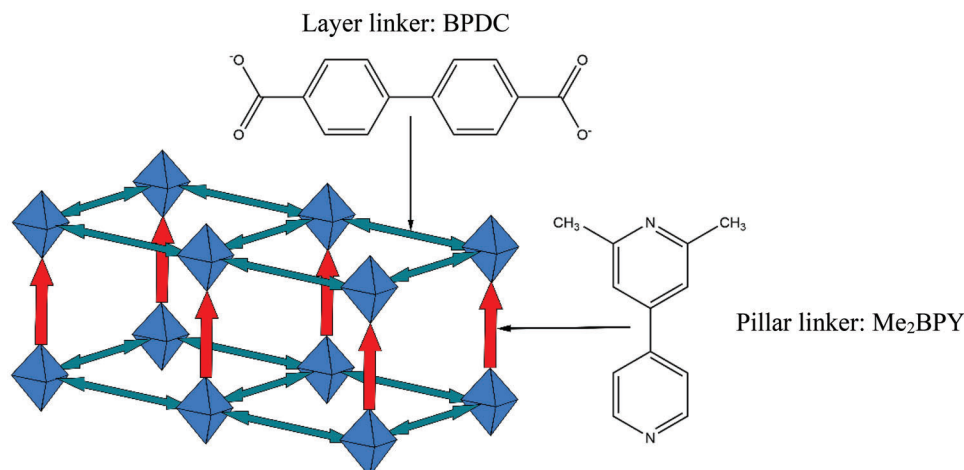


**Figure 1.** Idealized 3D scheme of a pillared-layer SURMOF with perfect alignment of the pillar linkers. The design goal of this study is to align the asymmetric pillar linkers (one-sided red arrows) within a layer. The symmetric layer linkers are shown by double-sided dark cyan arrows, while the SBU of the SURMOF are represented by blue octahedrons. The electric fields induced by dipole alignment are detectable but far too small to drive the assembly process toward a highly ordered state. In present experimental realizations, up / down ratios deviate only a few percentage points from random alignment.

semiconductors, such as photovoltaics<sup>[6]</sup> and organic light-emitting devices.<sup>[7]</sup> In previous work, the huge potential for framework materials, covalent organic frameworks<sup>[8]</sup> and metal-organic frameworks<sup>[9,10]</sup> (MOF) for the realization of NC materials has been analyzed using theoretical methods.<sup>[11,12]</sup>

Recently, a multilayered NC material has been experimentally realized<sup>[13]</sup> through the layer-by-layer (LbL) deposition of surface-coordinated metal-organic framework (SURMOF).<sup>[14,15]</sup> In general, MOFs are a class of nanoporous designer materials where the individual building blocks, namely metal clusters, also referred to as secondary building units (SBUs), and organic linkers, can be chosen from a combinatorial list of options. The LbL technique for SURMOF synthesis involves alternating deposition and rinsing cycles to stack 2D layers aligned in the *x-y* plane upon one another, iteratively thickening the SURMOF in the *z*-direction to maintain high degree of alignment and defect suppression with unprecedented spatio-temporal control over the dynamic growth.<sup>[15,16]</sup> Using appropriately functionalized substrates in connection with two different types of linkers, a so-called pillar-layered MOF can be assembled, with the layer linkers (dicarboxylic acids) aligned in the *xy*-plane and the pillar linkers aligned along the *z*-direction, perpendicular to the substrate. **Figure 1** depicts an idealized representation of the design goal of this investigation, where the pillar linkers and their dipole moments are perfectly aligned. In such a scenario, the dipole moments carried by the pillar linker collectively induce an intrinsic electric field.<sup>[17]</sup> In case of linker alignment, the field is macroscopically measurable, e.g. through surface core-level shifts using X-ray photoelectron spectroscopy;<sup>[18]</sup> in addition, the non-centrosymmetric structure gives rise to second-harmonic generation.<sup>[13,19]</sup> Unfortunately, the alignment of dipoles in a parallel arrangement is energetically unfavorable (so-called center symmetry trap).<sup>[20]</sup> Therefore, in order to yield aligned dipolar asymmetric linkers, large distances between the pillar linkers and a difference in binding energy has to be realized, which favors an arrangement with parallel pillar linkers.

Immediately after immersion of the substrate, linkers will bind to the “empty” SBU sites and yield a random orientation of pillar linkers. Subsequently, successive binding-unbinding processes will take place. In the presence of a substantial difference in “up” and “down” binding energies, unbinding effects will be more likely for the configuration with the lower binding energy. Since the following re-binding process is again random, these binding-unbinding events will cause an “annealing” of the system and eventually yield a fully aligned system.

In previous work,<sup>[13]</sup> a copper-based SURMOF (Cu(BPDC)(Me<sub>2</sub>BPY)) fabricated using methyl-functionalized, asymmetric bipyridine pillar linkers (denoted as Me<sub>2</sub>BPY, see Figure 1), the maximum up-down ratio of linker orientation (schematically illustrated with red arrows in Figure 1) amounted to merely 52:48. The reasons for this low degree of orientation have remained unclear.<sup>[13]</sup>

In order to resolve this inconsistency and for developing a rational strategy to obtain asymmetric Cu-based SURMOFs with a high degree of alignment, a thorough analysis on the dependence of degree of alignment on the different factors governing LbL-growth is required. In the present paper, we use a theory-driven multiscale modelling approach which combines ab initio calculations for binding energies for individual pillar linkers and master equations and kinetic Monte Carlo (kMC) simulations on the coarse-grained scale for the dynamics of MOF growth, to systematically improve the pillar linker alignment. The multiscale simulation reveals that the alignment of the pillar linkers is hindered by a kinetic limitation in the LbL process: even if a highly ordered alignment is thermodynamically favorable, a timescale separation in the reversible binding reaction, i.e., a fast-binding-slow-relaxation process, prevents the pillar linkers from reaching the highly aligned equilibrium state. To circumvent such kinetic limitation, we have screened a wide range of candidate pillar linkers, to identify design guidelines of the linker structure to facilitate significantly improved alignment.

## 2. Results

### 2.1. Rate Equation Model

We first present a simple rate equation model to understand the fundamental principles governing the growth process. To keep the analysis simple, dipole-dipole interactions (which are small as discussed later when introducing in the kMC model) are neglected. In the LbL process, the substrate with exposed SBUs (blue-cyan-colored xy-layer in Figure 1) is submerged in a solution containing an excessive amount of free pillar linkers. As long as the adlayer is in contact with the solution, reversible binding-unbinding reactions take place. The kinetics during the assembly of a monolayer of pillar linkers is considered. During the binding reaction, a free linker from the solution binds to the substrate in either the up or down configuration, occupying a vacant site on the 2D lattice of SBUs. Inversely, for the unbinding reaction, a bound linker can be released from the 2D lattice and returned to the solution, vacating a binding site on the substrate. The total number of accessible sites on the substrate is limited, whereas the supply of free pillar linkers is determined by the concentration in the solution. This process can be modeled by a set of ordinary differential equations:

$$\begin{aligned} \frac{dW_u}{dt} &= r_{f \rightarrow u} W_f (100\% - W_u - W_d) - r_{u \rightarrow f} \cdot W_u \\ \frac{dW_d}{dt} &= r_{f \rightarrow d} W_f (100\% - W_u - W_d) - r_{d \rightarrow f} \cdot W_d \end{aligned} \quad (1)$$

$$\frac{dW_f}{dt} = 0$$

where  $W_u$  and  $W_d$  represent the concentration (in percentage, within the interval [0,100%]) of linkers bound in the up and down configurations, respectively. Term  $W_f$  represents the concentration of free linkers and it remains constant.

In the dynamic system of (equation 1), the energy levels for a free linker, a linker bound upward, and a linker bound downwards can be defined as ( $E_f$ ,  $E_u$ ,  $E_d$ ), respectively, which are shown in Figure S1 (Supporting Information). The transition rates among these distinct energy levels are specified as:

$$r_t = \exp\left(-\frac{\delta E_t}{kT}\right) \quad (2)$$

where  $t$  corresponds to a transition from ( $f \rightarrow u$ ,  $f \rightarrow d$ ,  $u \rightarrow f$ ,  $d \rightarrow f$ ). The rate  $r_t$  is computed from the energy differences, e.g.  $\delta E_{f \rightarrow u} = E_f - E_u$ . The temperature  $t = 300$  K and  $k$  is the Boltzmann constant. A bound linker can reorient by consecutive unbinding-binding reactions, i.e., on-site flipping ( $u \rightarrow d$ ,  $d \rightarrow u$ ) is not considered.

Solving (equation 1) and (2) for  $t \rightarrow \infty$ , the system relaxes to a stationary state with a constant up-down ratio corresponding to the thermodynamic equilibrium. Because only energy differences (and not total energies) occur in the model, we can choose  $E_f = 0$ , and the up-down ratio is solely dependent on binding energy at both ends of the pillar linker, i.e., ( $E_u$ ,  $E_d$ ). For simplicity we assume  $E_u > E_d$  and write the binding energy as ( $E_{\text{strong}}$ ,  $E_{\text{weak}}$ ). Since the linker binding energies cannot be easily determined experimentally, we have computed ab initio binding energies as described in the Methods section. For the  $\text{Me}_2\text{BPY}$  linker from the reference,<sup>[13]</sup> we have computed ab initio binding energies of (0.62, 0.52 eV), which set the scale of the following investigation.

We note that these energies are computed in an implicit solvent model for EtOH environment, i.e., the entropic effects contributing to the binding free energy is neglected. The energies reported below should therefore be considered as relative energies with respect to this reference point. In the following, we have investigated a phase space for hypothetical pillar linkers with binding energies ranging from 0.2 to 0.8 eV which is in the range of ab initio binding energies from  $\text{CF}_3$ -functionalized bipyridine linkers to quinuclidine-based linkers. (Table S1, Supporting Information) The phase diagram in the ( $E_{\text{strong}}$ ,  $E_{\text{weak}}$ ) plane, along with the  $\text{Me}_2\text{BPY}$  reference system, is shown in Figure 2. The stationary state always results in a fully occupied layer of pillar linkers, such that the linker alignment is solely described by the up-ratio  $\eta_{\text{up}} = W_{u; t \rightarrow \infty}$  with the corresponding down-ratio ( $100\% - \eta_{\text{up}}$ ). The up-ratio in equilibrium is regulated by temperature: for fixed  $\delta E$ , an increase in temperature leads to reduced up-down differences. Shown in the inset of Figure 2, for a hypothetical linker with small  $\delta E = 0.06$  eV,  $\eta_{\text{up}}$  is relatively sensitive with respect to temperature, while for reference linker  $\text{Me}_2\text{BPY}$  with  $\delta E = 0.17$  eV, the  $\eta_{\text{up}}$  changes only slightly, even if the temperature is doubled from ambient conditions. Both systems exhibit a highly ordered linker alignment in this model.

The equilibrium phase diagram almost always features a highly ordered alignment. A diagonal contour of  $E_{\text{strong}} = E_{\text{weak}}$  marks the 50:50 line, i.e., a random distribution of “up” and “down” configurations. The reference contour for a 70:30 up-down ratio, a value which would be desirable to reach in the experiment, is parallel to the 50:50 contour. Regardless of the absolute values of the binding energy, as long as the linker is at least slightly asymmetric with  $\delta E = E_{\text{strong}} - E_{\text{weak}} > 0.05$  eV, a transition from random orientation to near perfect alignment is achieved, as indicated by the arrow in Figure 2.

### 2.2. KMC Model

For the bipyridine-based asymmetric linkers used in the previous assembly of NC SURMOFs,<sup>[11,13]</sup>  $\delta E$  amounts to 0.17 eV, and the equilibrium model would thus predict a highly ordered, well-aligned arrangement. However, experimentally a relative orientation of only 52:48 is observed, thus creating an apparent discrepancy. This inconsistency indicates that the pillar adsorption process is not determined by energetics alone, and we speculated that reaction kinetics come into play. In order to account for this consideration, we have implemented a more detailed theoretical descriptions of the LbL process, namely lattice-based kMC simulations of the growth of an individual layer, which capture the dynamics of reversible binding reactions occurring during the LbL SURMOF assembly.

kMC simulations have been successfully employed in simulating structure formation and reaction routes<sup>[21–23]</sup> in sub-atomic, atomistic, coarse-grained levels and the SURMOF assembly can also be approached via the atomistic and coarse-grained levels.<sup>[16]</sup> Here in a coarse-grained representation of the linkers, our kMC model considers a substrate with 2D lattice of binding sites, consistent with the scheme in Figure 1. In the first step of the SURMOF-forming process, the asymmetric pillar linkers can bind to the undercoordinated SBU sites with their axis orientated perpendicular to the substrate, with either an up or

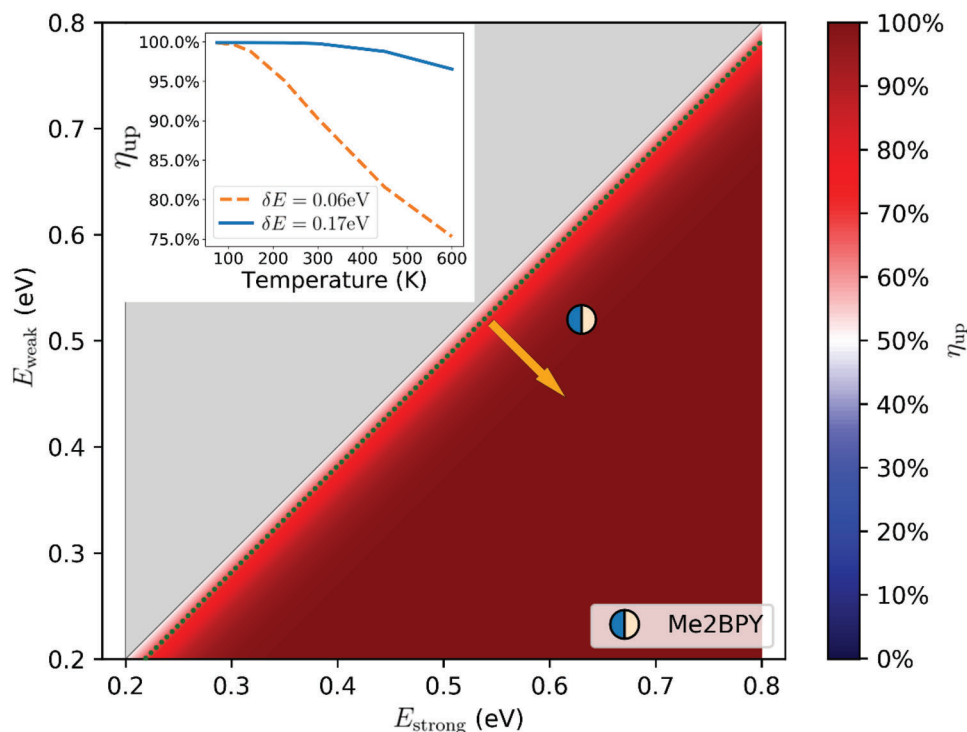


**Figure 2.** Phase diagram of pillar linker alignment in the master equation model in equilibrium at  $T = 300$  K. The linker orientation results from the relative binding energy to the SURMOF substrate. The diagonal solid boundary corresponds to  $E_{\text{weak}} = E_{\text{strong}}$ , as the upper half is marked forbidden by definition. The dark green dotted line indicates the contour at 70:30 up-down ratio. The fractional linker alignment improves in the direction of  $\delta E = E_{\text{strong}} - E_{\text{weak}}$  as indicated by the orange arrow. The circular marker corresponds to the computed energy values of the experimentally tested linker Me<sub>2</sub>BPY.<sup>[13]</sup> Based on the binding energies we would expect a near perfect ordering (>90%), but the experimentally achieved up-down alignment was observed only at  $\approx 4\%$ . If the temperature is increased, the 70:30 contour is moved in the direction of the orange arrow. The inset shows the relatively strong dependence of  $\eta_{\text{up}}$  on temperature for a hypothetical linker with  $\delta E = 0.06$  eV and weak temperature dependence for the Me<sub>2</sub>BPY linker.

down orientation. Since the bound state (with either up or down orientation) is energetically favorable over the unbound state, as the simulation proceeds, pillar linkers gradually cover the substrate in a stochastic process, reaching a random arrangement of up and down orientations. This situation is not static: on the microscopic level binding and unbinding events will occur which can flip the dipolar linkers between up and down orientations.

At any given time, an occupied lattice site can take the states (u, d) for linkers bound up / down with corresponding binding energy from  $(E_u, E_d)$ , whereas for a free site (f) the energy is  $E_f$ . In addition to effects considered in the master equation approach, a single linker binds to the substrate with a “chemical” binding energy that results from the interactions of the linkers with the SBU and the dipole-dipole interactions with other linkers already present in the system:

$$\begin{aligned} E_{\text{tot}} &= E_{\text{binding}} + E_{\text{dipole}} \\ E_{\text{dipole}} &= -\sum_i k_e d_i^{-3} \mu \mu_i \end{aligned} \quad (3)$$

where  $E_{\text{binding}}$  and  $E_{\text{dipole}}$  is summed over all occupied sites to define the total energy  $E_{\text{tot}}$ . In the dipole-dipole interaction,  $\mu$  is the dipole moment for the current lattice site where the linker is binding,  $\mu_i$  is the dipole moment for the bound linkers,  $d_i$  as the linker-linker distances from the current site to the  $i$ -th site, and  $k_e$  the Coulomb constant.

The system evolves by discrete events, where either an empty site is filled by a linker, or an occupied site releases a bound linker with a rate:

$$r_{ij} = \exp\left(\frac{-\delta E_{ij}}{kT}\right) / Z_i \quad (4)$$

where the partition function  $Z_i = \sum_j \exp(-\delta E_{ij}/kT)$  sums over all  $j$ -th reaction routes to switch among energy levels illustrated in **Figure 3**. The stochastic process in kMC uniformly and randomly samples all possible reactions from a given state to realize one of the candidate routes as a reaction event. The reaction time corresponding to such reaction event is thereafter sampled from a separate random number  $u \in (0, 1]$  as:

$$t' = t + Z_i \ln(1/u) \quad (5)$$

to propagate the simulation clock in kMC as  $t \rightarrow t'$ . Effectively, a reaction events which correspond to a drop in the energy landscape are sampled more frequently, with to a small increment in simulation time; while reaction event which leads to an increase in overall energy is rare, corresponding to a large increase in simulation time.

To take into consideration the solution environment, we include an entropic desolvation barrier in the energy landscape, see **Figure 3**. For a pillar linker to bind to the lattice site on the

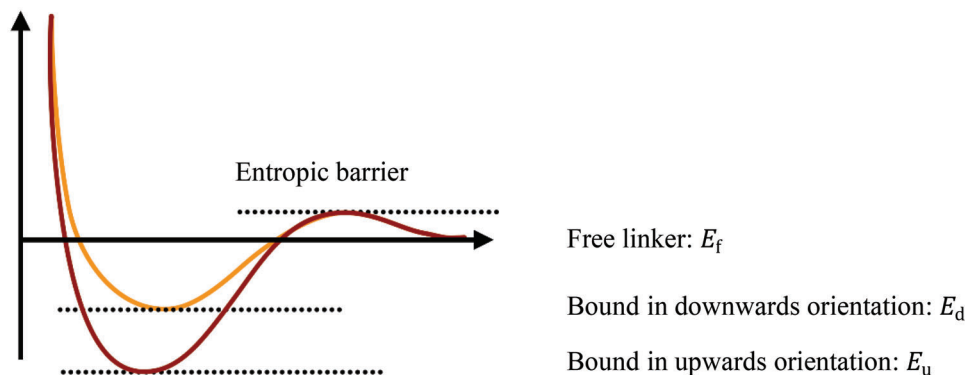


**Figure 3.** Scheme of energy landscape and energy levels of the up-down bound state with the entropic barrier.

substrate, the entropic barrier must be overcome followed by a drop into the energy well corresponding to the bound state. The rate of the binding reaction is determined by the entropic barrier height, which depends on experimental conditions, such as temperature, linker concentration, etc. The precise height of the entropic barrier is difficult to determine directly from simulations. Therefore, we have studied the importance of such barriers by investigating three different cases as low (0.025 eV), medium (0.05, 0.06 eV), and high (0.075 eV) entropic barriers. The introduction of an entropic barrier effectively equalized the reaction rates for upward-binding and downward-binding, which results in a random orientation of bound linkers, as observed experimentally. In fact, we found that for ambient temperature a fixed entropic barrier height at 0.05 eV the experimentally reported up-down ratio for the reference linker Me<sub>2</sub>BPY can be reproduced. The effect of temperature regulated barrier heights is discussed in the (Supporting Information). Importantly, when the height of the entropic barrier is lowered to zero, the kMC equilibrium agrees with the equilibrium phase diagram in Figure 2.

In contrast to the equilibrium case, where the up-down ratio is solely dependent on  $\delta E$ , we find a strong kinetic limitation of the growth process when employing the kMC model. In the kMC time series data (see Figure 4), a quick occupation of the substrate is followed by a long-standing intermittent state with a constant up-down ratio near 50:50, before recovering toward the equilibrium linker alignment obtained from rate equations. The duration of this intermittent state varies strongly with the average binding energies of the linkers. For a fixed  $\delta E = 0.05$  eV, the kMC time series of the up-down ratios corresponding to low, medium, and strong average binding energies show exponentially prolonged kinetic trapping in an intermittent state in Figure 4. With increasing average binding energy, the residence time in the intermittent state is extended by 10 orders of magnitude.

If the time used for a single cycle in the LbL process becomes shorter than this residence time, the linker adlayer will not be able to reach the energetic minimum. In the experimental LbL process, each cycle of linker deposition proceeds in a time interval of typically several minutes, followed by a rinsing step. After each cycle the subsequent layer of SBUs is deposited on top of the pillar linkers bound in the previous step. After deposition of the SBUs, the orientation of the underlying linkers is fixed. In order to simulate the experimental process, in the kMC simula-

tions a final snapshot is taken after a predetermined relaxation time. As discussed above, for experimentally relevant times this state corresponds to an intermittent state far from equilibrium. While we cannot compute exactly the relation between the experimental relaxation time and the kMC cut-off time, we find that for entropic barriers with heights of 0.05 eV the experimentally observed phenomena can be well described. From the long duration of the transient periods (see Figure 4) we conclude that the experimental system is always trapped in some intermediate state. For further analysis we set the duration of the kMC simulation to a value which reproduces the 52:48 up-down ratio reported for the Me<sub>2</sub>BPY linker in the previous experiments. In principle, longer SURMOF synthesis times would be able to alleviate the kinetic limitation of the up-down ratio. However, using long times for the individual cycles is impractical when dozens of layers need to be deposited. The changes in linker alignment with longer relaxation time are discussed in Figure S4 and S5 (Supporting Information).

From the finite-time kMC snapshots, the order parameter  $\eta_{\text{up}}$  can be retrieved for all hypothetical linkers *in the phase space of* ( $E_{\text{strong}}, E_{\text{weak}}$ ). We find that this new phase diagram is drastically different from what was obtained for the equilibrium case, demonstrating the importance of kinetic limitation. However, for a biased linker orientation, the dipoles they carry should induce an intrinsic electric field, which in return regulates the alignment of newly bound linkers in the adlayer through dipole-dipole interactions, also contributing to the overall linker alignment. To estimate the dipole induced linker alignment, we compared the phase diagrams with and without dipole-dipole interactions in Figure S3 in (Supporting Information) and Figure 5. Due to large lattice spacing in the SURMOF of  $\approx 2$  nm for the nearest neighbor pillar linkers, the dipole-dipole contribution is limited such that even for a substrate with a perfectly pre-aligned linkers, up-down bias in the next layer that results from the dipole interactions is <3%. We conclude that the dipole-dipole interactions play only a marginal role for linker alignment, and we have omitted the dipole contributions since the near random linker alignment is primarily a result of the kinetic limitation.

In Figure 5 for finite-time kMC calculations the kinetic limited region is highlighted, the white area indicates that the up-down ratio for a majority of the phase diagram is trapped in a state with random linker alignment. In order to illustrate an experimentally

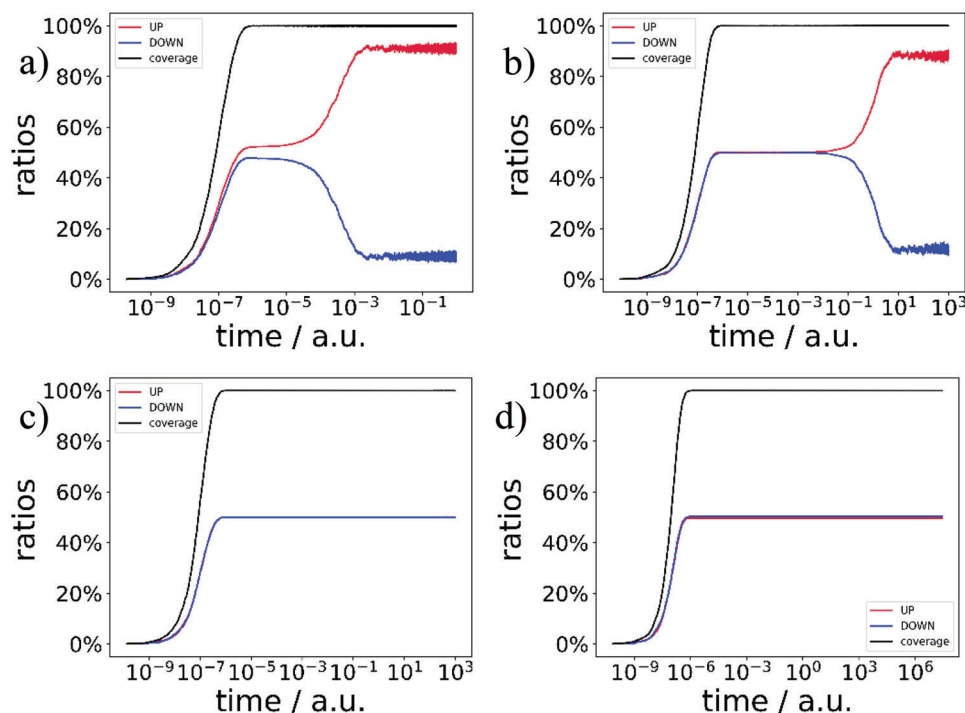


**Figure 4.** Two-stage transition for hypothetical pillar linkers with average up-down binding energy of a) 0.2, b) 0.4, c) 0.75, and d) 1.0 eV, while  $\delta E$  is fixed at 0.05 eV preferring up-binding. The time series for ratios of linkers bound in up-configuration, in down-configuration, and the total coverage of the substrate is shown in red, blue, and black color. The two-stage transition for the linker alignment can be decomposed into a fast occupation of the substrate corresponding to simulation time up to  $10^{-6}$  to reach a constant up-down ratio in an intermittent state, and a recovery from the intermittent state to the equilibrium. With increasing average binding energies, the residence time in the intermittent state is exponentially extended, kinetically trapping the up-down ratio around 50:50.

desirable scenario, we also show the line corresponding to 70:30 up-down ratio as “good alignment” in the phase diagram. Also, this line differs dramatically from the line obtained for the case when equilibrium is reached. The 70:30 reference line is divided into two segments: for small binding energies the 70:30 line coincides with the equilibrium boundary; for hypothetical pillar linkers with binding energy at  $\approx 0.4$  eV, the 70:30 line under kinetic limitation bifurcates from the equilibrium case (diagonal), to be “folded” to a horizontal line.

We can summarize the results of the kMC model as follows: The kinetic limitation of linker alignment results from a fast-binding-slow-relaxation mechanism, that is, a separation of time scales for the reversible binding reactions. Free linkers from the solution rapidly bind to the SURMOF substrate to fill all available binding sites with random linker orientations. The unbinding rate for the energetically disfavored orientation is low due to a large energy barrier, which is the sum of the binding energy and the entropic barrier. As a result, the unbinding reaction only very slowly vacates misaligned linkers from the substrate, which are immediately re-occupied by a second binding reaction, again in a random orientation. Therefore, many slow reactions are required to reach thermodynamic equilibrium. Despite the fact that there is a significant difference in the binding energies, the separation of time scales in the relaxation process to reorient the linkers, which is  $\approx 5$  orders of magnitude slower than a binding reaction, may lead to a layer with random orientation. This time scale separation is exem-

plified in the kMC time series data, in Figure 4 and Figure S4 (in Supporting Information).

To derive linker design rules from these observations, we must consider that the SURMOF growth cannot occur when the binding energy is too weak. For instance, the SURMOF does not grow with a fluorine-functionalized bipyridine linker ( $F_2$ BPY, with binding energy at 0.35 eV). Thus, for the current discussion, we have adopted the practical limit of 0.35 eV as the lower boundary for binding energies which can result in SURMOF growth. Summarizing the kMC snapshots in the phase diagram in Figure 5, along with experiment inputs, the data points in the phase diagram fall into 4 distinct phases (light blue labels):

- No SURMOF growth due to too low binding energy: Due to insufficient description of the solution environment, in the kMC simulations we cannot account for the cases where weakly binding linker fails to bind to the SBU in the MOF. However, from the experiment, the reference linker as fluorine-decorate bipyridine ( $F_2$ BPY, with binding energy  $\approx 0.35$  eV) does not grow the SURMOF. For  $E_{\text{weak}} < E_{\text{strong}} < 0.35$  eV, neither side binds to the SBUs, thus practically marks the upper limit for phase A at 0.35 eV.
- Highly ordered alignment in monolayers only: With  $E_{\text{weak}} < 0.35$  eV (binding energy of  $F_2$ BPY)  $< E_{\text{strong}}$ , the SURMOF cannot be synthesized in the experiment due to too low binding energy on the weaker half. Simulation results indicate

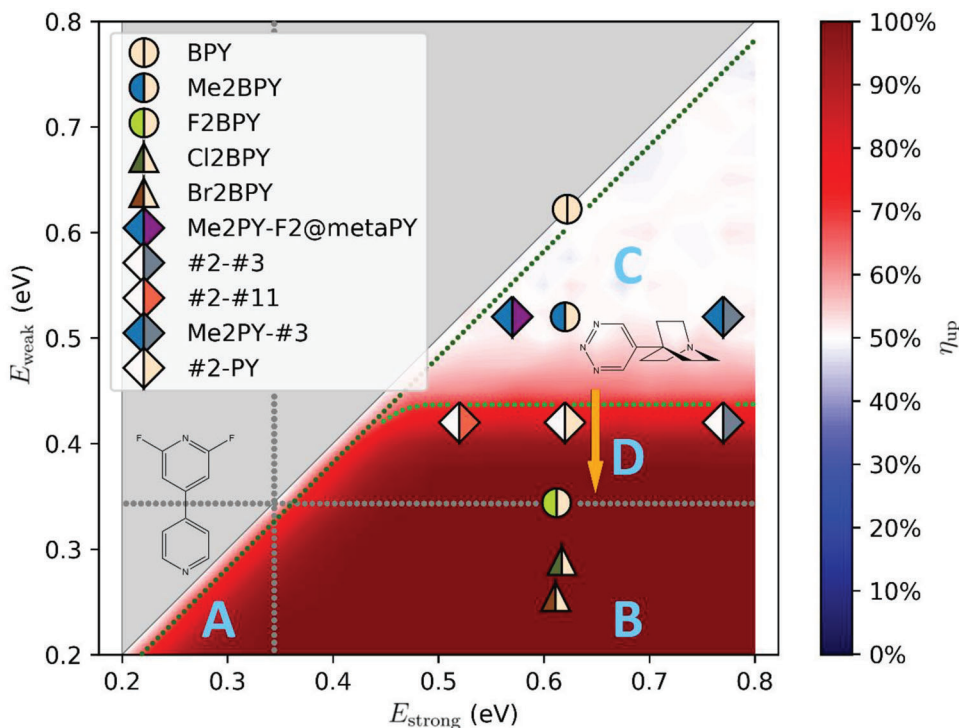


**Figure 5.** Phase diagram for linker alignment for hypothetical linkers with binding energy in the range of 0.2 to 0.8 eV for a finite time in the kMC model. Dashed lines indicate phase boundaries and phases are alphabetically labelled in light blue. The diagonal solid boundary marks the line  $E_{\text{weak}} = E_{\text{strong}}$ , above which no linkers exist by definition. The dark green boundary marks the 70:30 line as reference from equilibrium; the light green boundary indicates the “folded” 70:30 line which also considers the kinetic effect. Circular markers correspond to experimentally tested linkers, i.e., BPY, Me<sub>2</sub>BPY, and F<sub>2</sub>BPY. The hypothetical linkers of Cl<sub>2</sub>BPY and Br<sub>2</sub>BPY, as an extension to the experimentally tested halogen-functionalized BPY linkers, are indicated by the triangular markers. Theoretically proposed linkers are illustrated by diamond markers. The binding energies for all linkers are taken from ab initio calculations as strong-weak combination of separate “half-linkers”. Half-linkers with weaker binding energy are color-coded by the left side of the marker, and half-linkers with stronger binding energy are color-coded by the right side. For instance, among the halogen-functionalized BPY linkers the stronger binding side always correspond to pyridine, in light-salmon color; for a collection of triazine-including linkers as #2-#3, #2-#11 and #2-PY, the weaker binding side always correspond to 1,2,3-triazine, in white color. The variation of the stronger binding side moves the marker left-right in the phase diagram, while the variation of the weaker binding side moves the marker up-down. To design a linker with improved alignment from random to highly ordered, the critical factor is the binding energy of the weaker half-linker, indicated by the direction of the orange arrow. The linker structure of F<sub>2</sub>BPY is overlaid on the 0.35 eV critical boundary for successful SURMOF growth; one of the proposed linkers 1,2,3-triazine / quinuclidine which has high predicted up-down ratio  $\approx 70:30$ , is overlaid in the phase diagram, over the orange arrow for critical transition from kinetic limited to high linker alignment.

- a highly ordered linker alignment is achieved, because the stronger side of the linker can bind, but the next layer will not grow.
- C. Kinetically limited linker alignment: For large enough binding energy ( $E_{\text{weak}} > 0.35$  eV) but an insufficient energy difference, or too strong binding ( $E_{\text{weak}} > 0.42$  eV), the system remains in a kinetically trapped intermittent state with random orientations. Compared to phases A and B, the SURMOF grows, however the linker alignment is poor.
- D. Highly ordered linker alignment in SURMOF: For large enough binding energy ( $0.35$  eV  $< E_{\text{weak}} < 0.42$  eV) and significant binding energy difference  $\delta E > 0.05$  eV, a good linker alignment is achieved and the SURMOF should grow well.

The following consideration determine the position of the lines separating these 4 phases in Figure 5: In the equilibrium case,  $\delta E = E_{\text{strong}} - E_{\text{weak}}$  determines the up-down disparity, while for the kinetically limited case, the average binding energy defined as  $(E_{\text{strong}} + E_{\text{weak}})/2$  controls kinetic trapping. Since these

two energy factors are linearly correlated, the phase diagram is divided by linear boundaries. As discussed for the “good alignment”, the 70:30 line is drawn in the phase diagram in two linear segments. The “good alignment” for binding energies  $< 0.4$  eV is solely dependent on  $\delta E$ , whereas in the kinetic limited case, the linear dependence between average binding energy and  $\delta E$  makes  $E_{\text{weak}}$  the critical control variable for the linker alignment in separating phases C and D. The boundary between phases A and B is phenomenologically drawn at 0.35 eV, determined from the binding energy for F<sub>2</sub>BPY linker which fails to grow the SURMOF. Between phases B and D, the 0.35 eV threshold distinguishes a successful SURMOF growth from the formation of only a monolayer. The experimentally observed linker Me<sub>2</sub>BPY is located in phase C, subjected to kinetic limitation. These theoretical and practical boundaries enclose a “good” region in which pillar linkers successfully grow the SURMOF ( $0.4$  eV  $< E_{\text{weak}} < 0.42$  eV), but also align well with the smallest possible amount of binding energy on the weaker end, while the stronger end must secure a  $\delta E > 0.05$  eV.

### 2.3. Linker Design

To systematically design novel pillar linkers for improved alignment, we have considered candidate linkers with a chemical composition similar to the Me<sub>2</sub>BPY linker (see Figure 1) reported in the experiment.<sup>[13]</sup> In this molecule, the nitrogen atom on the para- site of each pyridine-based half-linker can bind to the SBU. Modifications on the ortho- and meta-sites can change the binding energy to the SURMOF substrate, however ab initio calculations for the binding energy for the complete linker with various ortho- and meta- modifications reveal that the binding energy via coordination to the SBU is determined mostly by modifications made on the ortho-site since they are capable of modulating the local electron density within the aromatic ring and nitrogen heteroatom more efficiently. Modifications farther than the ortho- groups have no substantial influence on the binding energies (< 0.04 eV). As a result, the candidate linkers can be considered as comprising two independent binding units, which can be designed as separate modules. The independent modules are designated as “half-linkers” to construct the complete linker with arbitrary  $E_{\text{strong}}$  and  $E_{\text{weak}}$  choices. Ab initio calculations indicate the energy difference between a complete and a half linker is negligible at  $\approx 0.001$  eV. To explore the chemical space of candidate half-linkers to reach a binding energy in the “good” region, we have developed an automated ab initio workflow for calculating the binding energy of half-linkers on the SURMOF substrate (details in Supporting Information). A library of candidate half-linkers with binding energies ranging from 0.4 to 0.8 eV are depicted in **Figure 6**. The binding energies of short-listed half-linkers are laid out in **Table 1**, and a comprehensive list of ab initio binding energies for all calculated linkers is included in Table S1 (Supporting Information).

The candidate half-linkers in Figure 6, represent two categories: pyridine-based (Figure 6a) and non-pyridine linkers (Figure 6b). For the modifications of pyridine-based linkers, we followed an approach similar to reference<sup>[24]</sup> to introduce electron-donating and electron-withdrawing functional groups as symmetrical pairs at the ortho- and meta- sites in order to fine-tune the binding energy via the nitrogen-SBU coordination. In Table 1, the pyridine-based linkers are designated as X-Y, where X represents the modification of the meta- group and Y represents the ortho- group (see Figure S6, Supporting Information). For Y = [H], the electron-donating groups X = -NH<sub>2</sub>, -SH, and -OH increase the binding energy by maximum of 0.04 eV compared to X = [H], whereas the electron-withdrawing groups X = -F and -Br reduce the binding energy on the nitrogen site by 0.04 eV. By substitution on the ortho- site from Y = [H] to Y = -NH<sub>2</sub>, -SH, and -OH, the electron-donating groups improve linker-SBU binding; however, their effects are counteracted by steric repulsion due to the increased size of the modified groups. Alternatively, with Y = -F and -Br, both the electron-withdrawing effect and the steric effect reduce the binding energy. For Y = -CH<sub>3</sub>, the large meta-modifications as X = -F etc. results in ortho- -CH<sub>3</sub> rotation to facilitate a reduced binding energy compared to X-Y = [H]<sub>2</sub>C. We find that pyridine-based modifications always result in a reduced binding energy compared to pristine pyridine.

Most binding energies of non-pyridine half-linkers are lower than that of pristine pyridine (Table 1). The only exception is the quinuclidine half-linker (#3 in Figure 6), which is similar

to 1,4-diazabicyclo[2.2.2]octane, i.e., DABCO. The DABCO pillar linker, which is frequently employed for synthesis of pillar-layered SURMOFs, maintains a very strong binding to the SURMOF ( $\approx 0.79$  eV). With the quinuclidine half-linker (binding energy of 0.77 eV) it sets the highest record among all candidates of half-linkers. For non-DABCO cases, the binding energies are close to the pristine pyridine half-linker, with the exception for the 1,2,3-triazine (#2 in Figure 6). There, the binding energy reduces to 0.4 eV with minimal penalty in steric effect. To estimate the EtOH solvent environment, we have used an implicit solvent model, increasing the dielectric constant from vacuum to 24.3 in EtOH (see Experimental Section): We find that most binding energies for the candidate half-linkers are reduced, in a range from 0.03 eV (for quinuclidine) to  $\approx 0.16$  eV (for O-[H]). An exception to this trend is 1,2,3-triazine, whose binding energy in EtOH is slightly higher (by 0.02 eV) than what was obtained in vacuum. We conclude that solvent effects at the continuum level do not significantly affect the ranking of the half-linkers in terms of binding affinity.

Through the systematic linker design, the hypothetical pillar linker composed of 1,2,3-triazine as the weaker end (with binding energy at 0.4 eV) occupies the desirable region in the phase diagram in Figure 5. The kMC predicted alignment for this linker improves from having little preference (52:48 up-down ratio) for the original Me<sub>2</sub>BPY to approximately 65:35 for triazine-based linkers. For a collection of triazine-based linkers, including triazine / oxazole (#2-#11), triazine / pyridine (#2-PY), and triazine / quinuclidine (#2-#3) our model predicts consistent highly ordered linker alignment.

### 3. Conclusion

To summarize, we have combined ab initio calculations with kinetic Monte Carlo simulations to develop a multiscale model for the dynamic growth of a pillar-layered SURMOFs. We find that the state of the system is not only governed by the energy difference between the different orientations of the linker. Instead, we found that during the fast-binding reaction, the introduction of an entropic barrier dictates a quick linker occupation of the substrate with random orientations. However, with slow-relaxation, the linker alignment is kinetically trapped in such intermittent state far from equilibrium. Due to such time scale separation in the reversible binding-unbinding reaction, the linkers, such as methyl-functionalized bipyridine, cannot reach a highly ordered alignment in the experimentally accessible timescales.

The results of our analysis as contained in the phase diagram depicted in Figure 5 allows us to derive strategies to reduce the kinetic limitation and improve alignment ratios beyond what has been realized previously. We find that a critical minimal binding energy at  $\approx 0.4$  eV is required for both orientations of the linker to make SURMOF growth possible. Moreover, a critical maximal binding energy at  $\approx 0.42$  eV is identified for the weaker binding side of the candidate linker, beyond which a kinetically limited linker alignment traps the up-down ratio around 50:50. Finally we require a  $\delta E = E_{\text{strong}} - E_{\text{weak}} > 0.05$  eV to achieve a reasonable alignment in the equilibrium.

To systematically construct the pillar linker to fit the binding energy criteria, a pillar can be divided into a stronger and a weaker binding half-linker, with individual half-linker optimized



independently. In this modular approach for the pillar linker design, the binding energies of various candidate linkers are calculated on a SURMOF substrate, utilizing an automated quantum mechanics workflow. For pyridine-based half-linkers, substituting H-atoms on the ortho- site with electron-donating or -withdrawing functional groups invariably reduces the binding energy, whereas on the meta- site, any modifications have insignificant contributions  $< \approx 0.04$  eV. Among the non-pyridine options, the quinuclidine half-linker offers the highest binding energy at 0.8 eV. In the phase space, the candidate half-linkers form a grid, and the 1,2,3-triazine / quinuclidine combination is placed in the region with a predicted  $\approx 70:30$  alignment. Synthetic efforts for the newly proposed linkers are underway, but due to the non-conventional linker composition at this point in time test experiments cannot be carried out.

A pillar-layered SURMOF with programmable linker alignment presents a highly promising approach for manipulating the intrinsic electric fields in an ordered 3D solid-state material. In principle in a multilayered compound, the field direction and strength in each layer can be individually tuned, to open unprecedented capability in engineering sophisticated polarized pore structures with ordered field intensities in a 3D framework.

#### 4. Experimental Section

The development of master equations and kMC models were implemented with in-house codes. The SURMOF was presented as a 3D lattice with lattice constants as 2 nm x 2 nm x 2 nm in x, y, and z directions. Since the reversible binding reactions can be described by discrete energy levels, the corresponding binding energy values used for the kMC simulations can be represented as ab initio binding energies, in the present study using density functional theory (DFT). The binding energy for the pillar linker was calculated as the energy difference between the total energy of the linker-on-substrate complex and the sum of the energies of the isolated pristine SURMOF substrate and the free linker, from identical dimensions for the simulation box of 2 nm x 2 nm x 5 nm.

First, the isolated linker were optimized using B3LYP functional<sup>[25–28]</sup> with def2-SVP basis set<sup>[29]</sup> in TURBOMOLE 7.4.1,<sup>[30]</sup> with Grimme D3 dispersion correction<sup>[31]</sup> with BJ damping.<sup>[32]</sup> The bulk Cu(BPDC) (Me<sub>2</sub>BPY) SURMOF layer was optimized with Perdew-Burke-Ernzerhof (PBE) functional<sup>[33]</sup> in the plane-wave DFT (PW-DFT) using the Vienna Ab initio Simulation Package (VASP) 5.4.4,<sup>[34]</sup> with Tkatchenko-Scheffler method with iterative Hirshfeld partitioning.<sup>[35–37]</sup>

Subsequently, the linker was joined collinearly to the paddlewheel of the SURMOF (linker-on-substrate complex), and the single point energy difference of the binding was determined. PW-DFT was used to calculate the energies separately for the isolated substrate  $E_{\text{layer}}$ , the isolated pillar linker  $E_{\text{linker}}$ , and the linker-on-substrate complex  $E_{\text{complex}}$ . Binding energy was defined as  $E_{\text{complex}} - E_{\text{linker}} - E_{\text{layer}}$ . This binding energy corresponds to a negative value as the linker-on-substrate was energetically favored. In the context of the manuscript, the reference to the term “binding energy” corresponds to the absolute value of binding energy.

To sample the most probable binding mode of a particular candidate of the pillar linker with regard to the SURMOF substrate, both the rotation angle of the linker and its distance to the copper atom in the SBU in the completely aligned Cu(BPDC) (Me<sub>2</sub>BPY) SURMOF were scanned (see Figure S8, Supporting Information). It was to be noted the pillar-layered SURMOFs cannot be fabricated for arbitrary metal-clusters and in our current investigation the SBU was limited to Cu-based SBUs. In the majority of candidate linkers, the optimal binding energy was obtained when the rotation angle was  $\approx 45^\circ$  with respect to the oxygen atoms in the SBU, for the quinuclidine linker the optimal binding energy was found at 0 rotation. (Figure S9b, Supporting Information) The linker-SBU distance were sam-

**Table 1.** Ab initio binding energies of short-listed half-linkers. Structures of half-linkers with respective labels are depicted in Figure 6. We note that solvent effects tend to shift all binding energies in the same direction, i.e., the energy differences are hardly affected.

Identifier for the half-linker	Binding energy [in eV]		Identifier alias in the naming convention in Figure 5
	in vacuum	in implicit EtOH	
[H]_[H]	0.68	0.62	PY, BPY
[H]_C	0.63	0.52	Me <sub>2</sub> PY, Me <sub>2</sub> BPY
[H]_F	0.35	0.34	F <sub>2</sub> BPY
[H]_Br	0.34	0.29	Br <sub>2</sub> BPY
[H]_Cl	0.32	0.26	Cl <sub>2</sub> BPY
[H]_CF3	0.18	0.16	TFM <sub>2</sub> BPY
F_C	0.53	0.46	F <sub>2</sub> @metaPY
C1 = CN = NN = C1	0.40	0.42	#2
C1CN2CCN1CC2	0.80	0.77	#3
C1 = COC = N1	0.59	0.52	#11

pled in the range 0.22 to 0.3 nm PW-DFT data were fitted with a Morse potential and yield the lowest (global) binding energy (see Figure S9a in Supporting Information).

Solvent effects on the binding energy of the linker to the SURMOF substrate in the ab initio calculations were investigated using an implicit solvent model (VASPsol). The ethanol (epsilon of 24.3<sup>[38]</sup>) solvent environment corresponding to the experiment SURMOF synthesis conditions was utilized, see Figure S10 (Supporting Information).

All DFT calculations were performed using an automated workflow which was described in detail in Supporting Information.

Additionally, ab initio structure optimization and binding energy calculation was also performed for the reference Me<sub>2</sub>BPY on a substrate containing BPY pillar linkers, to compare the influence in binding energy between a symmetric substrate and a pre-aligned substrate. The minimal ( $< 0.02$  eV) difference during the switching of alignment in the substrate validates the calculation in using a single SURMOF unit cell.

#### Supporting Information

Supporting Information is available from the Wiley Online Library or from the author.

#### Acknowledgements

M.L., M.K., W.W, and C.W. gratefully acknowledge funding from the Deutsche Forschungsgemeinschaft (DFG, German Research Foundation) through the Excellence Cluster “3D Matter Made to Order” (EXC-2082). M.E. acknowledges funding from DFG within the Research Training Group “Scale Bridging Methods of Computational Nanoscience” (GRK-2450). M.L. thanks the computing resources provided by the high-performance computing grid of HoreKa. The authors would like to thank for excellent conversations from Dr. Tobias Schlöder for on the SURMOF layer configuration and from M.Sc. Zhiyun Xu and Dr. Alexei Nefedov on the experimental configuration of the SURMOF layer-by-layer synthesis, respectively.

Open access funding enabled and organized by Projekt DEAL.

#### Conflict of Interest

The authors declare no conflict of interest.

## Data Availability Statement

The data that support the findings of this study are available from the corresponding author upon reasonable request.

## Keywords

kinetic limitation, metal-organic frameworks, non-centrosymmetric, virtual materials design

Received: March 8, 2023  
Revised: April 5, 2023  
Published online:

- [1] G. J. Ashwell, P. D. Jackson, W. A. Crossland, *Nature* **1994**, 368, 438.
- [2] B. B. Ivanova, M. Spittler, *J. Phys. Chem. A* **2010**, 114, 5099.
- [3] G. D. Boyd, R. C. Miller, K. Nassau, W. L. Bond, A. Savage, *Appl. Phys. Lett.* **1964**, 5, 234.
- [4] W. J. Alford, A. V. Smith, *J. Opt. Soc. Am. B* **2001**, 18, 524.
- [5] O. R. Evans, W. Lin, *Acc. Chem. Res.* **2002**, 35, 511.
- [6] R. Chakraborty, P. K. Rajput, G. M. Anilkumar, S. Maqbool, R. Das, A. Rahman, P. Mandal, A. Nag, *J. Am. Chem. Soc.* **2023**, 145, 1378.
- [7] K.-H. Lin, G.-J. A. H. Wetzelaer, P. W. M. Blom, D. Andrienko, *Front. Chem.* **2021**, 9, 800027.
- [8] H.-S. Xu, Y. Luo, X. Li, P. Z. See, Z. Chen, T. Ma, L. Liang, K. Leng, I. Abdelwahab, L. Wang, R. Li, X. Shi, Y. Zhou, X. F. Lu, X. Zhao, C. Liu, J. Sun, K. P. Loh, *Nat. Commun.* **2020**, 11, 1434.
- [9] C. Wang, T. Zhang, W. Lin, *Chem. Rev.* **2012**, 112, 1084.
- [10] J. Enríquez, C. Manquian, I. Chi-Duran, F. Herrera, D. P. Singh, *ACS Omega* **2019**, 4, 7411.
- [11] G. Nascimbeni, C. Wöll, E. Zojer, *Nanomaterials* **2020**, 10, 2420.
- [12] V. Obersteiner, A. Jeindl, J. Götz, A. Perveaux, O. T. Hofmann, E. Zojer, *Adv. Mater.* **2017**, 29, 1700888.
- [13] A. Nefedov, R. Haldar, Z. Xu, H. Kühner, D. Hofmann, D. Goll, B. Sapotta, S. Hecht, M. Krstić, C. Rockstuhl, W. Wenzel, S. Bräse, P. Tegeder, E. Zojer, C. Wöll, *Adv. Mater.* **2021**, 33, 2103287.
- [14] O. Shekha, H. Wang, T. Strunskus, P. Cyganik, D. Zacher, R. Fischer, C. Wöll, *Langmuir* **2007**, 23, 7440.
- [15] D.-H. Chen, H. Gliemann, C. Wöll, *Chem. Phys. Rev.* **2023**, 4, 011305.
- [16] Q. Zhang, Y. Pramudya, W. Wenzel, C. Wöll, *Nano Mater.* **2021**, 11, 1631.
- [17] F. Würthner, *Acc. Chem. Res.* **2016**, 49, 868.
- [18] M. Gärtner, E. Sauter, G. Nascimbeni, A. Wiesner, M. Kind, P. Werner, C. Schuch, T. Abu-Husein, A. Asyuda, J. W. Bats, M. Bolte, E. Zojer, A. Terfort, M. Zharnikov, *J. Phys. Chem. C* **2020**, 124, 504.
- [19] W. M. K. P. Wijekoon, S. K. Wijaya, J. D. Bhawalkar, P. N. Prasad, T. L. Penner, N. J. Armstrong, M. C. Ezenyilimba, D. J. Williams, *J. Am. Chem. Soc.* **1996**, 118, 4480.
- [20] J. Lu, X. Liu, M. Zhao, X.-B. Deng, K.-X. Shi, Q.-R. Wu, L. Chen, L.-M. Wu, *J. Am. Chem. Soc.* **2021**, 143, 3647.
- [21] M. Esmaeilpour, S. Jana, H. Li, M. Soleymanbrojeni, W. Wenzel, *Adv. Energy Mater.* **2023**, 13, 2203966.
- [22] M. Andersen, C. Panosetti, K. Reuter, *Front. Chem.* **2019**, 7, 202.
- [23] X. de Vries, P. Friederich, W. Wenzel, R. Coehoorn, P. A. Bobbert, *Phys. Rev. B* **2019**, 99, 205201.
- [24] H. Kühner, L. Leyen, Z. Hassan, C. Wöll, S. Bräse, *ChemPlusChem* **2023**, 88, 202200425.
- [25] S. Grimme, *J. Chem. Phys.* **2006**, 124, 034108.
- [26] C. Lee, W. Yang, R. G. Parr, *Phys. Rev. B* **1988**, 37, 785.
- [27] P. J. Stephens, F. J. Devlin, C. F. Chabalowski, M. J. Frisch, *J. Phys. Chem.* **1994**, 98, 11623.
- [28] S. H. Vosko, L. Wilk, M. Nusair, *Can. J. Phys.* **1980**, 58, 1200.
- [29] A. Schäfer, H. Horn, R. Ahlrichs, *J. Chem. Phys.* **1992**, 97, 2571.
- [30] S. G. Balasubramani, G. P. Chen, S. Coriani, M. Diedenhofen, M. S. Frank, Y. J. Franzke, F. Furche, R. Grotjahn, M. E. Harding, C. Hättig, A. Hellweg, B. Helmich-Paris, C. Holzer, U. Huniar, M. Kaupp, A. Marefat Khah, S. Karbalaeei Khani, T. Müller, F. Mack, B. D. Nguyen, S. M. Parker, E. Perlt, D. Rappoport, K. Reiter, S. Roy, M. Rückert, G. Schmitz, M. Sierka, E. Tapavicza, D. P. Tew, et al., *J. Chem. Phys.* **2020**, 152, 184107.
- [31] S. Grimme, J. Antony, S. Ehrlich, H. Krieg, *J. Chem. Phys.* **2010**, 132, 154104.
- [32] S. Grimme, S. Ehrlich, L. Goerigk, *J. Comput. Chem.* **2011**, 32, 1456.
- [33] J. P. Perdew, K. Burke, M. Ernzerhof, *Phys. Rev. Lett.* **1996**, 77, 3865.
- [34] G. Kresse, J. Furthmüller, *Phys. Rev. B* **1996**, 54, 11169.
- [35] A. Tkatchenko, M. Scheffler, *Phys. Rev. Lett.* **2009**, 102, 073005.
- [36] T. Bučko, S. Lebègue, J. Hafner, J. G. Ángyán, *J. Chem. Theory Comput.* **2013**, 9, 4293.
- [37] T. Bučko, S. Lebègue, J. G. Ángyán, J. Hafner, *J. Chem. Phys.* **2014**, 141, 034114.
- [38] R. V. Shinde, A. R. Deshmukh, S. A. Ingole, A. C. Kumbharkhane, *J. Adv. Dielect.* **2019**, 09, 1950018.